Inspecting manufacturing precision of 3D printed concrete parts based on geometric dimensioning and tolerancing

Automation in Construction 117 (2020) 103233

Contents lists available at ScienceDirect

Automation in Construction

journal homepage: www.elsevier.com/locate/autcon

Inspecting manufacturing precision of 3D printed concrete parts based on geometric dimensioning and tolerancing

Jie Xu[a,b,*], Richard A. Buswell[a,*], Peter Kinnell[c], Istvan Biro[c], John Hodgson[c], Nikolaos Konstantinidis[d], Lieyun Ding[b]

[a] School of Architecture, Building and Civil Engineering, Loughborough University, UK
[b] ViSAC Center, School of Civil Engineering and Mechanics, Huazhong University of Science and Technology, Wuhan, China
[c] Wolfson School of Mechanical, Electrical and Manufacturing Engineering, Loughborough University, UK
[d] Concrenetics bvba, Parc Industriel de Tournai Ouest 2, Tournai, Belgium

ARTICLE INFO

Keywords:
3D concrete printing
Geometric dimensioning and tolerancing
Net-shape
Feature size
Tolerance
Additive manufacturing

ABSTRACT

The additive manufacture of parts using extrusion-based techniques such as 3D Concrete Printing (3DCP) offers an alternative to traditional moulding processes. The precision to which the desired shape can be produced, however, is limited by the extrusion process and layer thickness, exacerbated by the deformation that occurs in the wet material during manufacture. Quantifying manufacturing precision is a critical part of defining process capability and quality control procedures, but this has yet to be explored for these technologies. To address this, this paper presents the problem of evaluating the geometrical precision of manufactured parts and then proposes an approach based on geometric dimensioning and tolerancing (GD&T), commonly used in manufacturing. This is then applied in a case study in order to demonstrate the application of the technique for understanding and defining process capability, to enable more effective design rules that lead to greater confidence in the viability of part designs, and to provide the reliable performance metrics necessary for process improvement and control. The work concludes that the outlook for such techniques is positive and that the application will be beneficial in the future development of quality control procedures for 3DCP.

1. Introduction

Large-scale additive manufacturing processes for the construction sector have been under development internationally for the last 15 years [1]. Many are based on the extrusion of wet mortar in a process similar to Fused Deposition Modelling, where filaments are deposited layer by layer to form the desired object [2,3]. The processes are driven by a computer model used to generate the instructions required to control the additive manufacturing equipment. They remove the need for moulds, which offers a number of benefits including greater flexibility in design geometry and shorter lead-in times for part manufacture [4].

A dominant characteristic of additively manufactured parts is the native surface finish created by the sequential layering of the material, known as the 'staircase effect' [5]. Often this results in a post-processing overhead, in which the improvement of surface finish might be one operation required to make a part fit for purpose [6]. The left-hand image in Fig. 1 presents this problem for parts printed using cement-based mortar (3DCP) where the rheology of the material often results in extrusion diameters upwards of 10 mm and hence the precision of shape and surface forming is limited to about ± 5 mm (Fig. 1, centre image) [7]. This may not be problematic for some applications, such as the production of walls and columns [8–14], but can be where greater tolerances are required, as depicted in the right-hand image of Fig. 1, where the creation of part mating surfaces in joints in assemblies [15] or the reproduction of more precise features for aesthetic [16], or functional reasons [7,17] is required.

Surface quality and the precision in reproducing features is influenced by the nozzle diameter, shape and its orientation. The parts in Fig. 1 have been manufactured using a circular nozzle extruding material perpendicular to working surface. Changing the nozzle shape from round to rectangular as well as non-vertical nozzle orientation has been shown to yield improvements [18], as has the addition of a paddle to smooth the surface during extrusion [19] and varying the extrusion diameter [20]. Even with improvement strategies, however, key questions remain:

- How precise are the manufactured parts (or building elements)?

* Corresponding authors at: School of Architecture, Building and Civil Engineering, Loughborough University, LE11 3TU, UK.
E-mail addresses: J.Xu2@lboro.ac.uk (J. Xu), r.a.buswell@lboro.ac.uk (R.A. Buswell).

https://doi.org/10.1016/j.autcon.2020.103233
Received 16 September 2019; Received in revised form 13 April 2020; Accepted 16 April 2020
Available online 05 June 2020

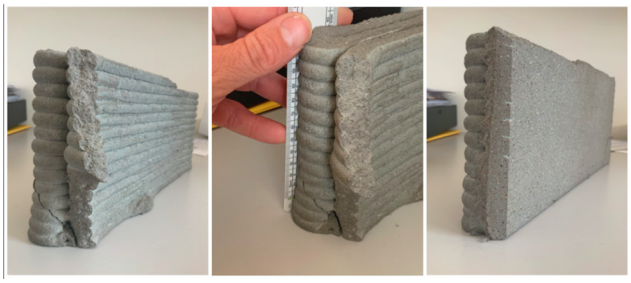

Fig. 1. Naturally striated surfaces of 3DCP parts on the left, the tolerances against a scale in the centre and an example of a ground flat surface on the right.

- Is this good enough for the application?
- Can the process be improved to deliver the required precision? And,
- to what extent does the part need modifying to make it fit for purpose?

The quality of manufactured parts is not only affected by the staircase effect, but deformation under self-weight during manufacture [21–23]. Additive manufacturing processes that use cement-based mortar have a complication in the significant role that the time dependent characteristics of cement hydration play in manufacture. Wet material must remain in a non-hardened state in order to facilitate extrusion and inter-layer bonding during manufacture, but this can lead to buckling of structures or plastic yielding towards collapse under the increasing hydrostatic loads [24,25]. The importance of these mechanisms has driven significant efforts in recent work: determining the rheological requirements of the wet material [26]; quantifying buildability [27,28]; and predicting structural failure [29,30] for controlling deformation behaviours. Undesirable effects can be exacerbated by poor control of material delivery and filament placement, and toolpath planning and so being able to benchmark process performance using measurement enables improvements to be trialled and evaluated systematically.

For those applications where producing the net-shape is beyond the capabilities of the 3DCP process, but where it is still beneficial to use 3DCP to produce a near-net-shape, further processing of the part is needed, commonly achieved through trowelling the surface, or the application of additional additive (e.g. rendering) or subtractive (e.g. milling) processes [3,31]. Understanding the process capability to enable the design of the near-net-shape part to accommodate a second process also requires systematic analysis, based on interrogation of manufactured parts, using a formal approach to measurement and evaluation.

Systematic methods for the assessment of manufacturing precision in 3DCP have not been investigated to date. However, there is a growing acknowledgement in the active community that this is important to:

- quantify and define process performance/capability;
- evaluate the quality of the features of a part; and,
- systematically interrogate processes, material and digital work flow to improve quality and performance.

This paper draws on methods used in manufacturing to address the problem of evaluating the quality and performance of 3DCP. It defines the nature of the problem, presents the background methods and then demonstrates the application using a case study of a well-known 3DCP process.

2. Background

The application of dimensional tolerances in construction has for many years been applied to cast part sizes and their spatial locations [32]. These are measured using traditional hand equipment such as manual measuring tape, theodolite and total station, shifting to digital equipment including laser distance measuring instrument, laser-based total station and 3D laser scanners. The dimensional tolerances for the creation of on-site formwork, specify the physical sizes of parts and their spatial locations within the entire building system [33,34]. However, dimensional tolerancing, as it relates to the finished building, to a large extent relies on experienced on-site craftsmen to custom-shape parts to work with each other, which is very different from the interchangeable parts required in manufacturing [35,36].

In manufacturing, Geometric Dimensioning and Tolerancing (GD&T) was established to provide standardised, comprehensive geometric measurement and tolerancing for all products. It is a symbolic language to specify the size, shape, form, orientation and location of features on a part, which reflects the actual relationship between mating parts, insuring proper assembly to improve quality and to reduce cost [37]. GD&T serves as a tool for mechanical designers and engineers to communicate design intent and provide a sound basis for geometric quality inspection, and is embodied in standards, such as the British Standards Institution (BSI) BS 8888:2006 [38], American Society of Mechanical Engineers (ASME) Y14.5 - 2018 [39,40] and China National Standards (CNS) GB/T 1182 - 2018 [41].

Integrated product and process design methods [42,43] and new types of tolerances [44] have been introduced in construction, but there remains little evidence of the implementation of GD&T methods within construction manufacturing, even though these methods have potential to contribute to the needed improvements in the efficiency of delivering the built environment [45,46].

The novelty of this work is the application of the GD&T system to support large-scale additive manufacture using cement-based materials. Parts are often bespoke, typically one-off and the precision of the manufactured geometry is affected by design and process parameters that are bound with highly time-dependent material properties that can be varied from seconds to hours or even days, making evaluating quality and understanding the factors that affect it challenging. This work provides a pathway through these factors in order to rationally define and understand process capability, and inspect and verify part quality. The approach could be applied to any construction manufacturing process, digitally driven or otherwise.

3. Problem definition

The final shape of parts that are manufactured using extrusion-based 3D concrete printing processes will vary due to combinations of:

- filament diameter and shape;
- layer height;
- tool path (strategy, pattern, tool orientation);
- material volume flow rate (in relation to tool velocity);
- inertia in the material at direction changes (nozzle velocity);
- material rheology, mix and process time dependency;
- part height;
- feature type, location and orientation on the part; and,
- shrinkage during hydration.

3DCP processes commonly manufacture bespoke parts, or elements of a building. These are often large objects and so reliability in manufacture is acutely important, not only in terms of productivity, but also in minimisation of waste.

The result is that there are many potentially variable manufacturing parameters driving the outcomes of the production of different design geometries which need to be fabricated correctly, with an acceptably low failure rate. In order to increase the likelihood that this is achievable in practice, the tolerances of the manufacturing process must be known so that they can be compared to the tolerances required by the

design to identify whether or not the process is capable of manufacturing a part that is geometrically fit for purpose. Therefore, a method is needed that can systematically determine process capability and, where appropriate, be used to interrogate that performance to understand how it can be improved. These methods need to be transparent, repeatable and standardised if processes and techniques are to be evaluated on a like-for-like basis.

The bespoke (certainly low volume) nature of 3DCP manufacture also means that monitoring the variation in precision of parts through the sampling of production is challenging in practice. Focusing on the ability of a 3DCP process to reproduce features, therefore, is one way to on which to base a useful quality measure because the reproduction of similar features could be tracked through inspection of many bespoke parts.

4. The GD&T framework for quantifying 3DCP process capability

In general, the basic features of common parts might include (but are not limited to) flat faces (planes), sharp corners, round or elliptical surfaces, curved edges, and holes. Two common features are the 'flat face' (plane) and the 'sharp corner' (edge), as both are key features for aesthetic quality and for the production of mating surfaces at interfaces between parts manufactured for assembly.

One challenging aspect is trying to navigate the many combinations of feature type, design, build orientation, material mix, batching, rheology, set control, process print speed, nozzle configuration, toolpath strategy, measurement options into a systematic and repeatable testing procedure. Fig. 2 presents such a framework based on GD&T.

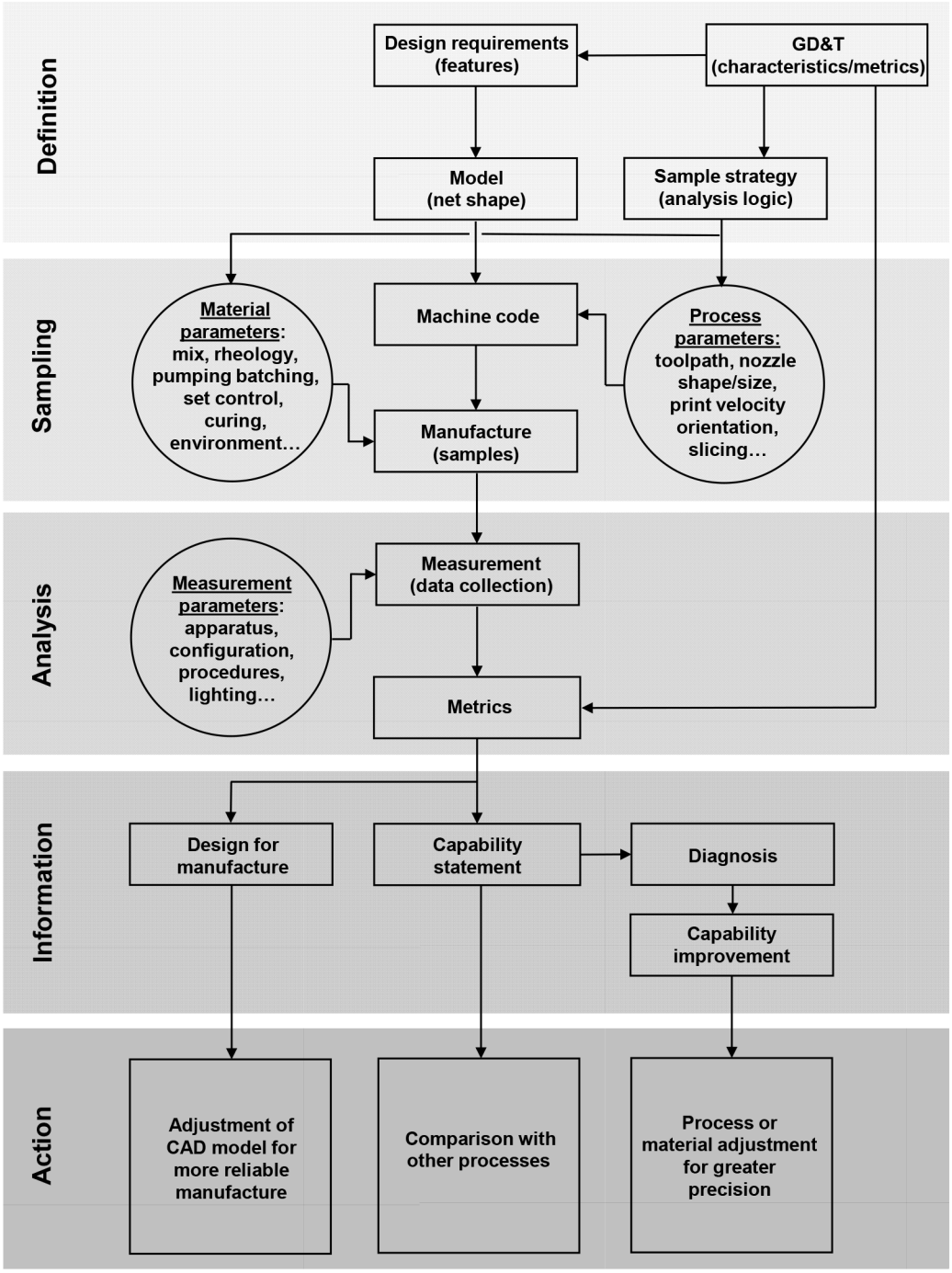

Fig. 2. GD&T framework for quantifying 3DCP process capability.

The rectangles represent key steps in the process, the circles represent the options for controlling the variability into the process, and the squares represent the actions informed by the information coming from the analysis. The approach breaks down into five stages from:

- *Problem definition*: the part geometry under inspection, which features and their geometric parameters are of interest, what types of tolerances to be specified and how they are calculated, and what sampling strategy you are going to use.
- *Sampling*: production of the parts in terms of various process and material parameters for inspection.
- *Analysis*: determination of measurement parameters and implementation, and then the derivation of the key metrics from the collected data.
- *Information*: generation of new information about design for manufacture, process capability statement and/or improvement based on the key metrics.
- *Action*: finally informed appropriate action, whether that is for process comparison, improvement, or to understand an aspect of the design for manufacture of a near-net-shape part.

Ultimately, when the capability of a process has been defined, the GD&T characteristics and metrics will be used to inform the processing of future part designs: either by providing the constraints of what is achievable; or to modify the net-shape geometry so that it can be manufactured in a two-step process where the near-net-shape is additively produced and the net-shape is achieved by applying some additional process.

4.1. GD&T geometric characteristics

There are fourteen geometric characteristics describing five types of tolerances that are routinely used by GD&T in manufacturing and these are listed in Table 1. A datum (axis or flat surface) is often used as a reference of location to specify those tolerances.

4.2. GD&T metrics

There are a number of metrics, or geometric error indicators, that could be applied for different geometric characteristics of tolerances. Four of the most useful (for *Form* and *Profile* tolerances) are the maximum positive and negative deviation errors, d_{pMAX} and d_{nMAX}; and the mean positive and negative volume deviation per unit area, $\overline{V}_p$ and $\overline{V}_n$, given by,

$$\overline{V}_p \approx \overline{d}_p * n_p/n, \tag{1}$$

$$\overline{V}_n \approx \overline{d}_n * n_n/n, \tag{2}$$

where n is the total number of points in the measured point cloud associated with the region of interest, n_p and n_n are the number of points that have positive and negative deviations respectively and $\overline{d}_p$ and $\overline{d}_n$ are the mean positive and negative deviation. By sampling manufactured parts, these metrics can be used establish the precision, accuracy and variability of a process or used to establish dependency on process, material or design parameters.

Form is evaluated using the difference between maximum positive and negative errors (for instance, *flatness* is represented by $\Delta d_f = d_{pMAX} - d_{nMAX}$), and the mean being calculated across a number of sample parts. Variation in the mean can be captured using 95% Confidence Intervals (CI) for assessing capability based on a sample of parts manufactured using the process. Because most parts manufactured using 3DCP are bespoke and have the need to be in tolerance 'every-time', 99% Prediction Intervals (PI) should be considered when designing a part for future manufacture, based on a previous sample. According to the scale of the selected sample, the CIs and PIs can be calculated using an applicable statistical distribution, e.g. Student's t distribution for a small sample. The mean positive and negative volume deviations are useful for evaluating *Profile* - the closeness of the part to the net-shape, and are treaded in a similar way.

Table 1
Geometric characteristics of tolerances.

Pertains to	Type of tolerance	Geometric characteristics
Individual feature only	Form	Straightness; Flatness; Circularity; Cylindricity
Individual feature or related features	Profile	Profile of a line; Profile of a surface
Related features	Orientation	Angularity; Perpendicularity; Parallelism
	Location	Position; Concentricity; Symmetry
	Runout	Circular runout; Total runout

Form: is a morphological control of an individual feature as a refinement of its size tolerance; all form tolerances apply to single or individual feature, independent of all other features and surface controls.
Profile: is a surface control which is the result of projecting the profile of an object on a plane or taking cross-sections through the object at various intervals; profile tolerance can be used to control the size and shape of a feature or the size, shape, orientation, and location of an irregular-shaped feature.
Orientation: is used to describe the angular relationship between features, which includes parallelism, perpendicularity, angularity, and, in some cases, profile.
Location: controls both the spatial location and the orientation of features, which significantly contributes to part function, part interchangeability, optimization of tolerance, and communication of design intent.
Runout: controls surfaces constructed around a datum axis and surfaces constructed perpendicular to a datum axis; it controls several characteristics of surfaces of revolution, such as coaxiality and circularity, as that surface is rotated about its datum axis. There will usually be a tolerance zone formed by two parallel planes or a cylinder specified to a toleranced feature. Feature size and shape falling within such a tolerance zone is recognized as qualified for desirable geometry and function.

5. Application case study

In this case study, GD&T based methods are applied to the inspection of the 3DCP process developed at Loughborough University. This is an extrusion-based additive manufacturing technique for fabricating solid geometries from a high-strength, cement-based mortar. The following section describes the specifics of the design of the test part, sample strategy, the 3DCP materials, the process and the measurement system. This is followed by the results of the analysis that demonstrate the method for evaluating process capability, feeding data back into design for manufacture and improving process performance.

5.1. Design of the test part and sample strategy

The test part design and sample strategy are formulated to identify the capability of the process to reproduce flat faces and edges as these are common aesthetic features but also critical for forming mating surfaces for interfaces between parts in an assembly and other elements of the construction. Two geometric characteristics from the GD&T library have been selected for this evaluation: *flatness*, to understand the quality of the (in this case) flat mating surfaces; and *profile*, to understand the quality of forming edges and to evaluate the proximity of the printed part to its net shape.

'Flatness' describes the inherent property of manufactured surfaces and can be located in any orientation, or location on the manufactured part. Flatness is not affected by the precision of the surface location on the part and so its datum is a plane that can be mathematically 'fitted' to the surface of the manufactured part. 'Profile' indicates the approximation degree of manufactured surfaces of a part to its expected geometry (design CAD model, the datum) and so the location of a feature does matter. Once these errors are understood for a process, they can be turned into manufacturing tolerances that can be used for monitoring the quality of manufactured parts.

The metrics of both flatness and profile are then used to measure process capability and so compare the effect of varying one process parameter (nozzle diameter and layer height in this case) on the precision of the printed part. They are then used to establish inflation metrics that can be used to modify the CAD net-shape model used to drive the manufacturing process, so that the printed part is appropriately sized for the incorporation of post-processing operations. This near-net-shape model is used in order that there is sufficient, material removed or deposited to allow for trowelling (a surface forming process), rendering (an additive process) and milling/grinding/cutting (subtractive processes) operations to be demonstrated.

Finally, the metrics are used to interrogate the process to identify areas that can be treated for the improvement of the printed precision and the test method in order to identify any problematic issues. In this example, the impact of toolpath configuration and an anomalous issue in the mix preparation one of the printed samples is used to demonstrate the sensitivity of the method to identify such problems.

5.1.1. Test part

The part design comprised several examples of both flat-face and edge features at varying inclines and angles so that the quality of their reproduction can be evaluated using the measures of flatness and profile. This led to a geometry depicted in Fig. 3, with nine flat faces (four vertical, three inclined and two horizontal flat faces) with nineteen corners (three vertical, four inclined and twelve horizontal corners). Two vertical flat faces, both 90° the working plane (F4 & F5), three inclined flat faces at 30°, 45° and 60° (F1, F2 and F3 respectively) and the top horizontal flat face (F6, 0°) were used in the analysis for surface flatness and profile. Seven corners were investigated for profile tolerance five: the five external corners (Ce1, Ce2, Ce3, Ce4 and Ce5); and the two internal corners (Ci1 and Ci2). The test geometry can be freely downloaded from [47].

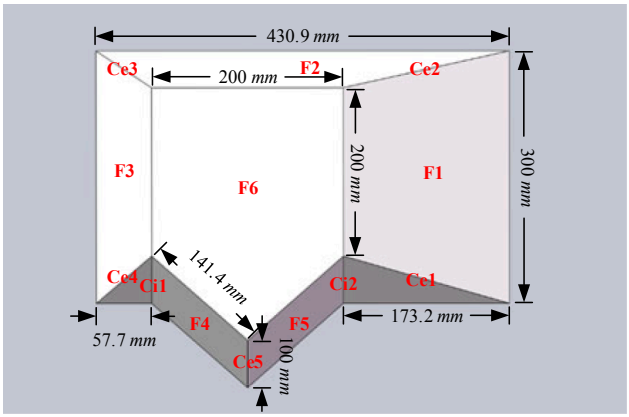

Fig. 3. Test part with nine flat faces and nineteen corners.

5.1.2. Sample strategy

In order to generate statistics that provide an indication of repeatability, several nominally identical examples must be manufactured. Three samples were selected for this study in order to demonstrate the approach, but larger a sample size is likely to be more robust in practice. The effect of changing a key process parameter (nozzle size/layer height) was investigated and so for each nozzle diameter tested (8 mm, 12 mm and 16 mm), a sample of three parts were manufactured. The nozzle diameter and the layer height was parametrically linked to diameter in the ratio of 0.52, giving respective layer heights of 4.2 mm, 6.3 mm and 8.3 mm and Groups 1, 2 and 3 respectively. Each Group can be used to quantify the repeatability and precision of the 3DCP process and comparison between groups provides insight into the effect of nozzle diameter on the attainment of the net shape.

5.2. Manufacturing apparatus

The 3D concrete printing apparatus is presented in Fig. 4. It is based on an ABB industrial robot with a circular nozzle out of PLA (polylactic acid) at its end effector. A pipe connects the printing nozzle with a screw (volume displacement) pump to convey the high-strength mortar (described in [48]) from the hopper to the nozzle.

The net shape model is converted to an STL file, which is sliced using Simplify3D software. Simplyfy3D was selected because it supports different types of 3D printers and can perform pre-print simulations before physical printing [49]. The tool paths used where a conventional perimeter outline with a diagonal hatching pattern. Two borders were printed and the internal hatching alternated at 45° between odd and even layers. The tools paths were converted to G-code and then transformed into robot code and simulated in RobotStudio (ABB Ltd.), and physically without materials prior to each print batch.

5.3. Material, batching and printing parameters

Each sample was made with a fresh batch of mortar. The mixing, batching and printing time were as consistent as possible in order to minimise the variations in material rheology. The concrete mix design used is presented in Table 2. The time between the addition of water and the printing during manufacture was kept constant to reduce effects from the changes in the rheology as the cement hydrates [23]. The mix was retarded to give an open time of at least 1 h for printing. Each batch was 20 l and one test part was manufactured per batch. It took approximately 20 min for mixing of the sand (diameter $\leq$1.18 mm), the powder (cement, fly ash and silica fume) and then adding the superplasticizer after the water with the retarder.

Just before the mixed concrete is placed in the pump, its static shear strength is measured by a shear vane apparatus, which is the same measurement method applied by Le et al. [49]. This helps to determine

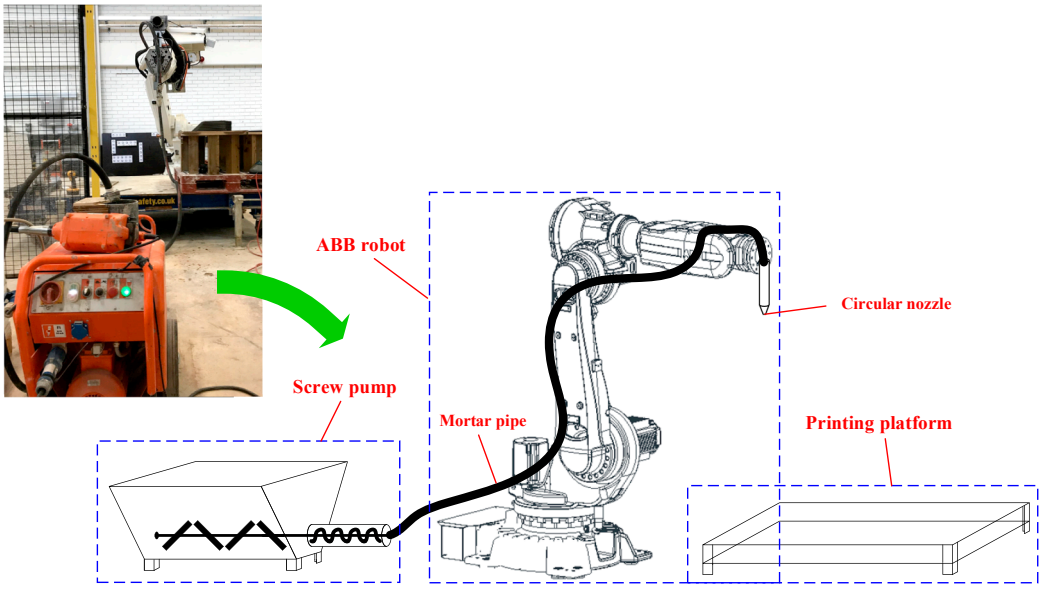

Fig. 4. Layout of the 3DCP apparatus system.

Table 2
Test material mix (given in grams per 20 litres).

Sand	Cement 52.5	Fly ash (Cemex 450-S)	Silica fume	Water	Superplasticizer (Spa Glenium 51)	Retarder (Delvo Stabiliser 10)
24,880	11,620	3,320	1,660	4,240	249	84

Table 3
Measured batch static shear strengths of the nine parts.

Group	1			2			3		
Part	1	2	3	4	5	6	7	8	9
Batch static shear strength (KPa)	1.08	1.08	1.08	1.09	1.08	1.13	1.16	1.09	1.09

similar rheological properties among different batches are achieved before each print. Table 3 gives the measured static shear strengths of the nine batches. Care was also taken to monitor the ambient conditions during printing (temperature and relative humidity) according to the lab thermal record and these remained reasonably constant (18 ± 1 °C, 50– 60%) for all except Part 4 and 5, when the temperatures were higher with lower humidity (25 ± 1 °C, 35– 45%) requiring a slight variation of superplasticizer dosage to maintain the target shear vane values.

Once prepared and checked, a small quantity of mortar is loaded and pumped anterior to the mixed concrete to wet the pipe and then the mortar is conveyed until the extruded material visually runs smoothly and steadily. As the part is manufactured, attention was afforded to the hopper of the pumps where occasional vibration was used to ensure the mobility of the mortar to flow into the pump rotor-stator without trapping pockets of air into the mix.

The mortar pump was run at the bottom end of its design flow rate to produce the samples. The resultant volume flow rates lead to deposition velocities at the nozzle between 100 mm/s and 200 mm/s to maintain flow and prevent the pump from overheating (at excessively low flow). The process parameters used are presented in Table 4.

5.4. Measurement

Contact metrology has been widely applied to inspect and verify feature tolerances, however, these methods can be difficult to set up and slow, especially when measuring large parts with abrasive surfaces. There has been a sustained effort to develop and apply optical 3D measurement techniques since the late 1980s and methods such as Time-in-flight sensors [50], laser triangulation scanning [51], interferometry [52], photogrammetry [53], laser tracking system [54], and structured light [55,56] have been developed. A comprehensive review of methods can be found in [57].

Structured light has been one of the most widely applied optical 3D measurement techniques because of its ease of implementation and fast full-field measurement by projecting a patterned field of light, usually a set of sinusoidal stripes, onto the surface being measured. The set of projected light patterns is then captured using a camera and combined to allow the projected field of light to be defined. Triangulation is used to determine the spatial position of pixels to represent points on the imaged surface, creating a point cloud. In this work, a Hewlett-Packard DAVID SLS-3 structured light scanner was used [58], pictured in Fig. 5a mounted on a robot.

5.4.1. Assessment of measurement accuracy

The accuracy of the DAVID scanner was assessed by following part two of the VDI/VDE 2634 standard for the assessment of optical 3D measuring systems. This involves positioning a ball-bar and flat plane artefact at a predefined set of seven poses within the scanner's measurement volume. For assessment of the DAVID scanner used in this work, a precision ground aluminium plate was used as the flat artefact. The plate provided a plane size of 500 × 400 mm, with a measured flatness ± 25 μm (measured using an LK Ultra coordinated measuring machine with a stated volumetric uncertainty of ± 1.75 + l/127 μm). The ball-bar used consisted of two precision ceramic balls, of 38 mm nominal diameter, spaced at a nominal distance of 300 mm. The distance between the balls and the diameter of each ball was calibrated by the supplier to a stated uncertainty of 1.1 μm and 0.8 μm respectively. During the scanner assessment all measurements were made with 0.3% outlier rejection as per VDI 2634, and the three parameters, SD, the error of the sphere spacing distance, P_s, the probing error and F, the flatness error were determined. Sphere spacing error, SD, is a measure

Table 4
Process parameters of Group 1, 2 & 3.

Group	Nozzle diameter/mm	Layer height/mm	Nozzle velocity/mm/s	Printing volume flow rate/ml/s	Part material dosage/L	Print time/min
1	8	4.17	200	5.5	9.2	28
2	12	6.25	100	6.2	9.2	25
3	16	8.33	100	10.2	9.2	15

of the ability of the scanner to measure length, and this was found to be 0.26 mm. Probing error, $P_{s,}$ represents the ability of the scanner to accurately measure small regions of the total measuring volume, and this was found to be 0.33 mm. Flatness error, F, represents the ability of the scanner to accurately measure points taken from a flat plane that spans the measurement volume, and this was found to be 0.31 mm. These values are all less than the expected and observed process variability.

5.4.2. Capturing part geometry

The measurement was taken at a material age of 6 days for Part 1– 6 yet 11 days for Part 7– 9 with a common lab curing condition of 20 ± 5 °C and 40– 60%. For each part, several scans from different directions were conducted to capture its geometry. This was implemented by using a robot to position the scanner in pre-set positions, ensuring that the entire surface of the part was measured with overlapping sections in adjacent scans.

Each scan is then processed and combined with the others using the *CloudCompare* software to produce the 3D point cloud of the part (Fig. 5b). The manual processing procedures include denoising, removal of background and surroundings, registration to align multiple scans taken from different views and finally fusion into a single point cloud presenting the entire shape of the test part. Notably, the registration is vital for achieving the correct spatial location of a target point cloud relative to its theoretical location, to ensure the accurate geometry of the part is obtained. Several methods [59] can be applied to accomplish a good registration. CloudCompare uses the Iterative Closest Point (ICP) method [60] where the objective in this study is to achieve a Root Mean Square Error (RMSE) difference of no more than a threshold of 1.0×10^{-5} mm between any two iterations during registration for each pair of overlapping point clouds. Here the RMSE stands for the virtual value of the average distance between any two compared points from their respective point clouds.

Subsampling of the final point cloud is then undertaken with a specific point-to-point distance as an acceptable subsampling precision for part cloud reduction; in this study the chosen precision for subsampling was 0.3 mm. Subsampling is useful as it reduces the computational cost associated with data processing and it yields a uniform point cloud that allows for good registration between the measured geometry of the test part presented by the point cloud data and the design geometry, a triangular mesh model created from a CAD model. Details of subsampling performance criteria can be found in [61].

5.4.3. Deriving feature errors

Flatness and profile can be evaluated by considering the geometric deviation errors between the actual feature state (data in a point cloud) and its ideal nominal geometry (a mathematical best fit, or the net shape as defined by the CAD model). The merged part point cloud needs to be ICP registered with the CAD model by the same RMSE (virtually average distance between the point cloud to the CAD model) difference threshold of 1.0×10^{-5} mm at an overlapping level of 70– 80%. On the test part used here, six flat faces are considered (F1 to F6), with five external corners (Ce1 to Ce5) and two internal corners (Ci1 to Ci2). Fig. 6 shows the net-shape CAD geometry with the point cloud data after the ICP registration. Boundaries between each area used in the analysis are marked with red and yellow dashed lines, defining the flat

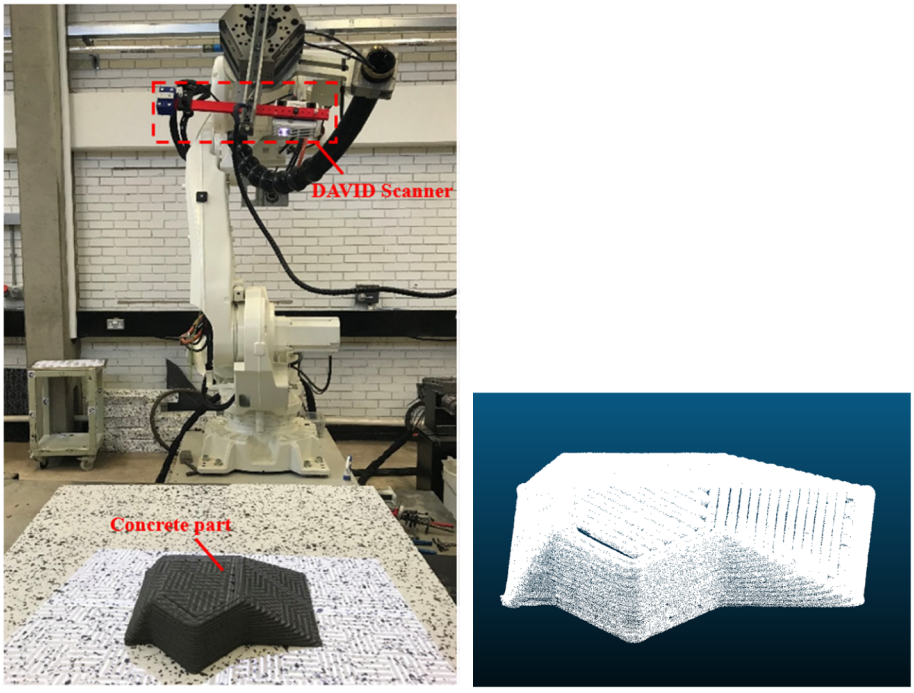

a b

Fig. 5. Measuring a printed part, a) deployment of a structured light scanner, b) fused point cloud.

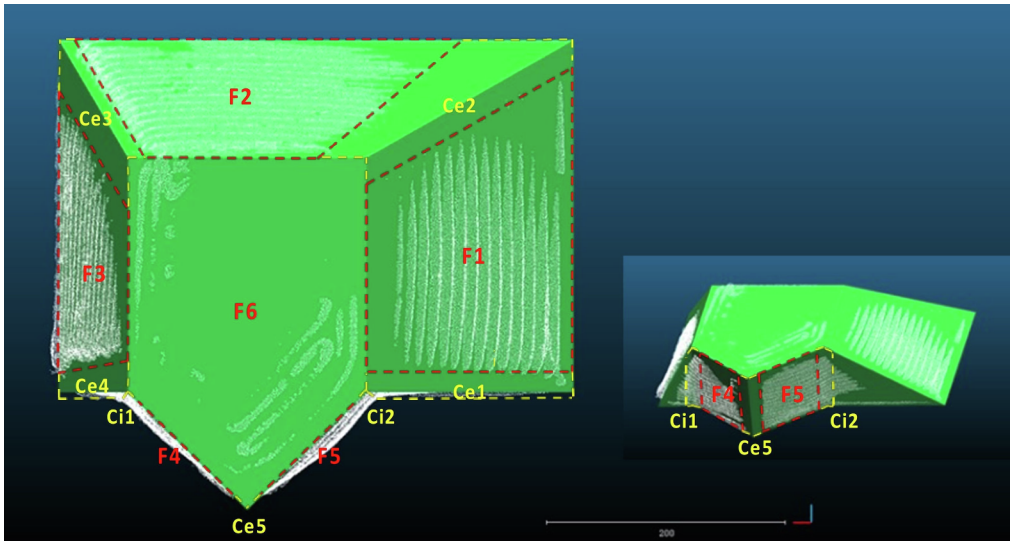

Fig. 6. The CAD model (green) and the point cloud (white) measured part after ICP registration, with the boundaries of the areas used in the analysis. (For interpretation of the references to colour in this figure legend, the reader is referred to the web version of this article.)

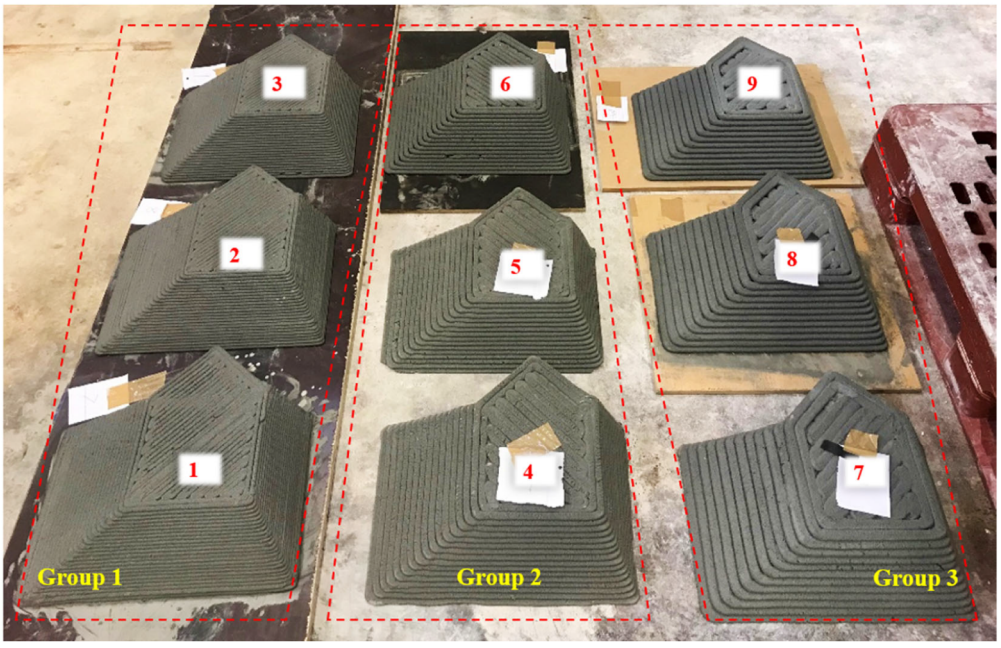

a

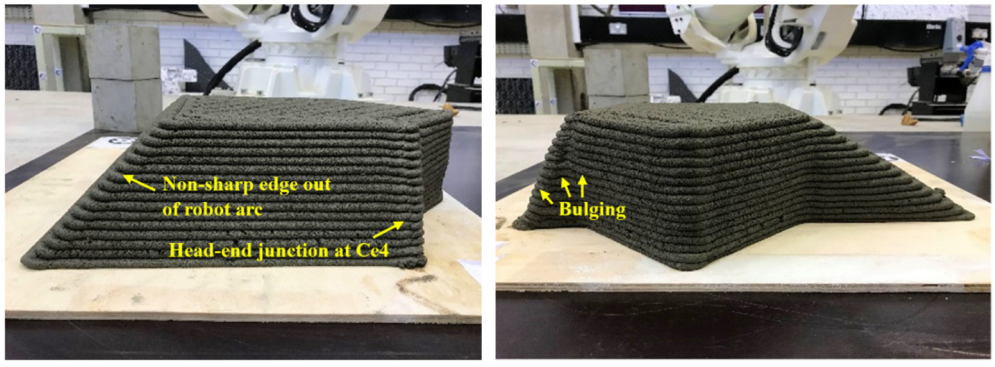

b

Fig. 7. Test parts manufactured, a) three groups of three parts where Group 1 used an 8 mm nozzle, Group 2 used a 12 mm nozzle and Group 3 used a 16 mm nozzle, b) surface details of a typical part.

Table 5
Flatness: quality of mating surfaces (combined for vertical, inclined and horizontal).

Flat faces	95% confidence intervals			99% prediction intervals		
	Mean difference 8 mm ⌀ (mm)	Mean difference 12 mm ⌀ (mm)	Mean difference 16 mm ⌀ (mm)	Mean difference 8 mm ⌀ (mm)	Mean difference 12 mm ⌀ (mm)	Mean difference 16 mm ⌀ (mm)
Horizontal	3.9 ± 0.5	5.3 ± 1.0	7.4 ± 0.7	3.9 ± 2.6	5.3 ± 4.8	7.4 ± 3.3
Vertical	6.1 ± 1.0	8.5 ± 2.3	6.9 ± 1.0	6.1 ± 4.3	8.5 ± 10.3	6.9 ± 4.4
Inclined	6.4 ± 0.9	8.4 ± 1.1	8.8 ± 1.0	6.4 ± 4.5	8.4 ± 5.3	8.8 ± 5.0
Overall	**5.9 ± 0.6**	**7.9 ± 0.9**	**7.9 ± 0.6**	**5.9 ± 4.0**	**7.9 ± 6.3**	**7.9 ± 4.2**

faces and vertices. Each area, in turn, is considered and the deviation between each point in the point cloud and the CAD model is measured normal to the surface of the model (implemented through the Cloud/Mesh Distance function in CloudCompare).

5.5. Results

Fig. 7a depicts all nine printed parts (Part 1– 9): Group 1, 2, 3 for the 8 mm, 12 mm and 16 mm nozzle diameters respectively. Visual inspection identified the following characteristics that may be undesirable in Fig. 7b: the arc path inherently used by the robot (in mechanical design) as it interpolates an edge resulted in rounded edges; the external corner Ce4, where the head-end junction of the perimeter toolpath on each layer is located and the subsequent bulging, distorting the forming of Ce4, Ci1 and F4. The approximate areas and number of points for each face and edge used in the analysis are given in Table A.1 in the Appendix for information.

5.5.1. Feature reproduction: creating flat faces

Table 5 gives the process capability statement for producing flat faces, for each of the three nozzle sizes. Looking at the overall mean differences, it can be seen that the errors are in the region of half the respective nozzle diameter in each case, which is to be expected since the reference plane is fitted to the surface. We might expect the order of decreasing performance to be in the horizontal, vertical and then inclined planes as long as the deformation related to the wet material rheology is well controlled, because inclined is the hardest to achieve a flat surface due to the tendency of the inclination to exacerbate the staircase effect.

However, for the 8 mm samples, inspection of the data in Table A.2 shows that the errors in Sample 2 (Part 2) were much worse than those in Sample 1 and 3 (Part 1 and 3). Further inspection of the part revealed much greater bulging, indicating that the rheology of the material was not consistent with the other two samples. We might conclude that the process creating Sample 2 (Part 2) went *out of control*. Likewise, the rheology problem also played a role in Sample 1 and 2 of Group 2 (Part 4 and 5) which also showed a significant increase in the uncertainty in the mean.

This inconsistency can be attributed to the slightly different material compositions of Part 4 and 5, where high environmental temperatures resulted in additional dosing of the mix with superplasticizer to maintain the target shear vane measurement during printing. This demonstrates that the approach is sensitive to unexpected influences on the process and can signal the need for further investigation to develop greater reliability in the processes. The horizontal surface is closer to what might reasonably be expected to be a straight line relationship between nozzle sizes and the resultant errors, as seen in Fig. 8.

5.5.2. Feature reproduction: creating edges

The profile errors of corners are calculated and treated in a similar way to the flat faces and presented in Table 6, data in Table A.3. Again, errors increase with nozzle diameter and are predominantly negative, illustrating the effect to the robot's arc movement at an edge and the consequential under-printing of external corners. This effect is reversed in internal corners where over-printing occurs.

These are important observations if secondary subtractive/additive processes are to be deployed as it suggests that the tool path at the corners must be modified to achieve the final net shape, which introduces an additional step in the generation of the machine instructions from the design geometry.

5.5.3. Proximity of the part to net-shape

Based on the data in Tables A.3 and A.4, Table 7 presents the mean deviations for all faces on the parts to give a condensed set of figures that could be used to compare process capability, or used to adjust the net-shape prior to printing in order to accommodate a second surface finishing process to take the part closer to the net-shape.

The feedback from the data suggests that if you want to trowel the

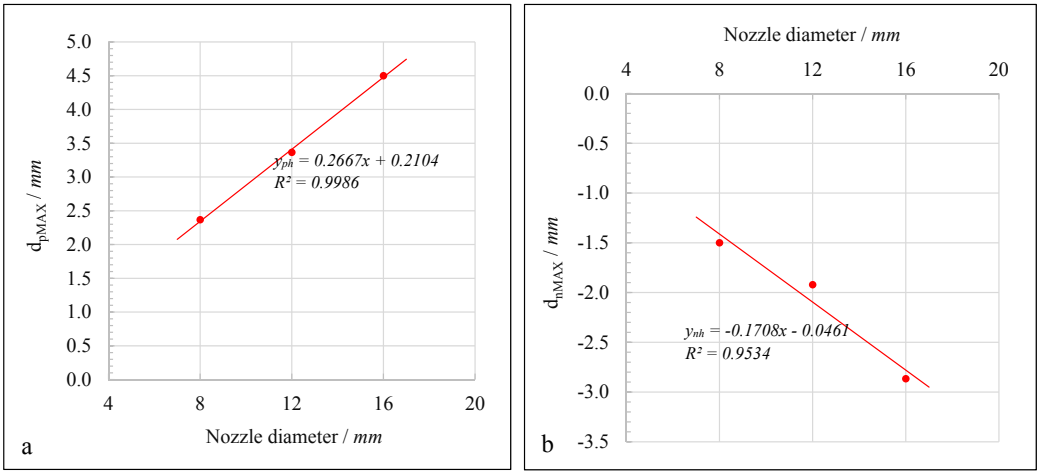

Fig. 8. Flatness errors variation of F6 along with the nozzle diameter, a) d_{pMAX}, b) d_{nMAX}.

Table 6
Profile - quality of reproducing edges (combined for external vertical, inclined and internal vertical).

Edges	95% confidence intervals			99% prediction intervals		
	Maximum error 8 mm ⌀ (mm)	Maximum error 12 mm ⌀ (mm)	Maximum error 16 mm ⌀ (mm)	Maximum error 8 mm ⌀ (mm)	Maximum error 12 mm ⌀ (mm)	Maximum error 16 mm ⌀ (mm)
Ext. vertical	−5.1 ± 1.1	−6.6 ± 2.7	−8.0 ± 0.7	−5.1 ± 5.4	−6.6 ± 12.9	−8.0 ± 3.5
Ext. incline	−4.5 ± 0.8	−6.4 ± 1.4	−8.4 ± 1.8	−4.5 ± 4.5	−6.4 ± 7.8	−8.4 ± 9.6
Overall	**−4.4 ± 0.7**	**−6.0 ± 1.1**	**−7.8 ± 1.2**	**−4.4 ± 3.8**	**−6.0 ± 6.7**	**−7.8 ± 8.0**
Int. vertical	6.7 ± 2.2	10.9 ± 3.9	7.5 ± 3.4	6.7 ± 10.2	10.9 ± 18.1	7.5 ± 15.4

surface to attain the net-shape, you need to ensure that the correct volume of material is deposited, given by $\overline{V}_p + \overline{V}_n$. It is evident from the data that the 16 mm nozzle diameter process is closer to this balance, and this might be the favourable process configuration in this case.

If additive methods are to be applied, then the part must not be larger than the net-shape in any dimension. In fact, it must be sufficiently smaller to accommodate the minimum thickness of the coating or rendering material. Here, deflating the model is necessary and the figures in Table 7 can be used to estimate this value by $d_{pMAX} + PI_{99\%} + T_m$, where $PI_{99\%}$ is the 99% prediction interval and T_m is the minimum thickness of the rendering material.

The opposite is the case for applying subtractive methods where the net-shape must be encapsulated completely by the net-net-shape where $|d_{nMAX}| + PI_{99\%}$ could be applied to estimate the required inflation of the net-shape prior to generating the toolpaths for manufacturing.

The deformation of the part under hydrostatic load might also affect the inflation estimates, further investigation of the data might be appropriate. Here, d_{pMAX} was sampled in 10 mm - thickness bands vertically across face F1, F2, F3 and F5 and observed as a function of height from the working plane, as presented in Fig. 9. This shows there is a substantial positive error, which tends to be at the greatest at about 20 mm–50 mm height, very much in line with observations by Wolfs et al. [21]. Notably, this appears less obvious in Group 2 which is likely to be due to the different material conditions in the manufacture of Part 4 and Part 5.

6. Discussion

The work presented here demonstrated a framework for evaluating performance capability and quality control based on GD&T principles. To limit the complexity of the analysis and minimise part variability, a consistent toolpath strategy was applied to all parts manufactured in this work. While best efforts were made to maintain constant material properties and a constant velocity of the printing nozzle to isolate these effects from the analysis, some variation did occur, which will also impact the resultant surface geometries. Higher volume flow rates were used in the manufacture of Group 1 to maintain minimum pump speed. This might affect shaping the deposited filaments and consequently the surface errors, this is difficult to quantify, although it can be assumed to be low for such a small nozzle diameter (8 mm) that constrains the difference it might make on the filament shape.

The curing time of Part 7– 9 is 5 days longer than the other samples, which may lead to 0.1– 0.2 mm additional shrinkage when compared to the other samples [62], but the effect in the results is negligible when compared to deviations generated by the other manufacturing factors. Parts 4 and 5 in Group 2 were subject to higher ambient temperatures which resulted in some additional superplasticizer being added to the mix to maintain constant shear vane measurements which were used as indicators of a similar rheological state. These unexpected inconsistencies were used to explore the effect on the measured errors.

3DCP, as with any additive manufacturing process provide process control challenge because of the inter-dependant relationship between materials, process and the target geometry, or design being manufactured. The challenge is to find ways to interrogate systems to unpick and identify causal factors. In this work, it has been shown that with carefully designed test geometries and standardised procedures, it is possible to allow for direct comparison of materials and process, which will underpin process bench-marking and production standards in the future. In practice in the wider community, the authors envisage a set of standard parts that can be manufactured in sample batches, that can be measured to generate data with which to determine many key factors that may influence process stability and part quality control.

For a quality control approach to be useful, it must be sensitive to a significant range of expected process variation. The proposed approach was shown to be sensitive enough to identify the effect of nozzle diameter on surface flatness and the material rheology on surface profile. It could identify the impact of toolpath configuration on the formation of edges and the effects of over-printing where the extrusion is stepped up to the next layer in the build. The evidence presented here suggests that modelling of expected behaviour could act as a useful indicator of influence on geometric quality. For example, once a parameter, related to process, material or design, is modelled into a relationship with a type of geometric error, any abnormal variation violating this model would indicate influences from other parameters.

6.1. Considerations for practical implementation

6.1.1. Measurement process

The point cloud of the 3D object is constructed by combining sets of point clouds capturing different sections of it, in a process called registration. This is achieved by matching the features captured by adjacent point clouds, using an iterative algorithm that minimises square errors to a predetermined threshold. The uniformity of data density within each of the captured point clouds is a key factor in achieving a

Table 7
Profile: closeness to net-shape.

Error: flat faces	95% confidence intervals			99% prediction intervals		
	8 mm ⌀ (mm)	12 mm ⌀ (mm)	16 mm ⌀ (mm)	8 mm ⌀ (mm)	12 mm ⌀ (mm)	16 mm ⌀ (mm)
Maximum positive	3.5 ± 0.5	4.9 ± 0.7	4.2 ± 0.4	3.5 ± 3.1	4.9 ± 4.8	4.2 ± 2.7
Maximum negative	−2.9 ± 0.3	−3.6 ± 0.6	−4.6 ± 0.6	−2.9 ± 2.2	−3.6 ± 3.8	−4.6 ± 3.8
Mean positive volume	0.62 ± 0.22	1.18 ± 0.43	0.74 ± 0.17	0.62 ± 1.39	1.18 ± 2.79	0.74 ± 1.09
Mean negative volume	−0.36 ± 0.09	−0.40 ± 0.17	−0.52 ± 0.13	−0.36 ± 0.56	−0.40 ± 1.07	−0.52 ± 0.80

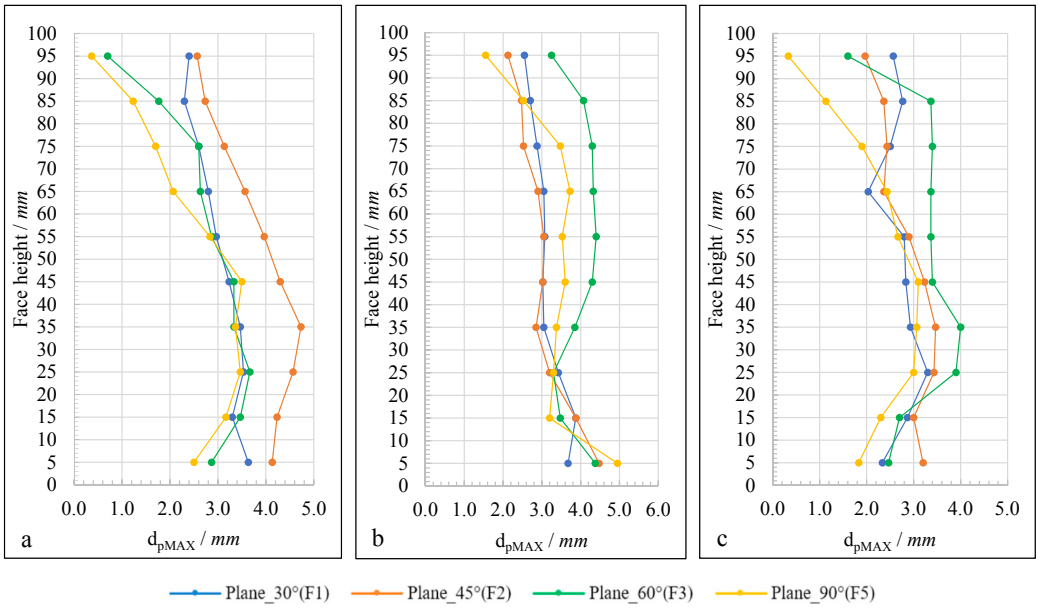

Fig. 9. Maximum positive deviation across face height for a) 8 mm (Group 1), b) 12 mm (Group 2) and c) 16 mm (Group 3) nozzle diameter parts for the inclined flat faces.

good registration of multiple point clouds. Non-uniformity in the points could lead to poor registration and require operator judgement and manual manipulation, increasing the errors in the resultant point cloud. As this is influenced by the light incidence angle of the scanner, care must be taken to define a set of optimum scan positions that enable the automation of registration. For practical applications, the accuracy of registration must be considered carefully to ensure the suitability of point cloud data. The RMSE difference threshold of 1.0×10^{-5} mm over the registered area in this work was quite enough to ensure the right position of each point in 3D space.

It must be also acknowledged that scale will affect the appropriateness of the measurement method, the spacing between the points in the cloud and ultimately what information can be extracted. Therefore, the part scale must also be considered when selecting the scanner to use and designing the measurement setup.

Selecting the appropriate scanner, and defining the optimum set of views can be achieved either by adequate adjustment through a representative specimen experiment, or by automatic assessment approaches that utilise scanner performance simulations and CAD geometry to digitally optimise scanner positioning [63,64]. Based on the above, automatic standardised procedures for data capture and processing can be deployed for efficient routine use and enable the performance comparison of different 3D printing apparatuses through measurement.

6.1.2. Design features

The test parts used in this work focused on the production of flat surfaces and edges, and explored a limited variation in process dimeters at a limited scale. Even from this reduced parameter space, a complicated relationship between the type of feature, machine and material properties, location of the part and part scale was found. Translating this into useful information, that can inform the design of parts, needs a sound understanding of the process. An expected benefit of feature-based extraction of data, that using GD&T allows for, is that future process investigations that adopt this approach, or publish point cloud data, can be more readily combined or compared.

6.1.3. Implementation of GD&T

Two tolerance measures were examined here, yet GD&T allows for a comprehensive set of features to be defined. The set of features used in this work prove the principle of the approach, and it is expected that in other studies more complicated geometries may exploit the significant flexibility of the full set of GD&T feature specifications that are possible. It is also anticipated that further work will explore other features found in architectural engineering and construction leading towards a standardised set of feature geometries for testing, calibration and performance monitoring.

7. Conclusions

3D concrete printing has been under development for > 15 years and the technologies are beginning to mature allowing them to move from an era of one-off fabrication of 'demonstrators' towards more routine deployment in manufacturing and construction. The typical scale of manufactured construction parts using 3DCP means that discarding parts that are not fit for purpose geometrically, or indeed in terms of mechanical properties, is extremely undesirable. The task of systematically evaluating the quality of the manufactured parts has not yet been routinely deployed, and this is in part because there are no published methods tailored to the idiosyncrasies of 3DCP manufacture.

This article has addressed the problem of quality assessment in 3DCP, and demonstrated that an approach based on GD&T is both practical and useful. A methodological framework based on GD&T was developed, and the approach was applied in a case study where a systematic evaluation was used to access the effects of materials and process on the geometric variability of manufactured parts. The case study allowed three key conclusions to be drawn:

- the GD&T principles routinely deployed in manufacturing can be directly applied to the additive manufacture of construction parts and together with corresponding metrics are sensitive enough to detect error variations related to process parameters and material rheology;
- GD&T allows part features to be considered in isolation, which enables the process calibration of 3DCP to be based on sampling and testing the reproduction of features instead of the entire part; and that,
- GD&T makes it possible to identify important factors that influence the formation of specific features when undertaking process calibration, in particular, deformation under self-weight causing

differences for flat faces, and effects caused by the robotic interpolation routine at corners; significantly causing under-printing for external edges and over-printing for internal edges.

The work demonstrated that GD&T can be used as part of a systematic approach to evaluate manufacturing tolerances; this provides clarity when interrogating process capability, which can lead to focused action to improve performance, and provide metrics for monitoring these gains. The investigation also demonstrated that for many practical purposes, the native manufacturing tolerances for 3DCP are impractically large. For 3DCP to be adopted and used more widely in construction, greater precision in manufacture will be a likely pre-requisite. 3DCP is likely, therefore, to be a near-net-shape process: i.e. be used to deposit an approximately shaped mass of material with further process steps to apply or remove material using more precise methods. GD&T provides the means to monitor and control these processes with reliable precision.

The knowledge developed here offers the underpinning for quality control procedures to be developed in this field as well as supporting potential new research areas for 3DCP such as design for manufacturing, process planning through mathematical optimization and in-process control techniques, tracking the research path found in conventional additive manufacturing.

Acknowledgements

This research is supported by: The National Key Research and Development Program of China (Grant number 2018YFB1306905) and the China Scholarship Council (CSC); the UKRI funded project, 'CAMBER - Concrete Additive Manufacturing for the Built Environment using Robotics' (Grant number EP/P031420/1; and the EPSRC funded projects, 'Collaborative Metrology Systems for High Value Manufacturing' (Grant number EP/L01498X/1), and 'Manufacturing integrated building components using digital hybrid concrete printing (HCP) technology' (Grant number EP/S031405/1). We would also like to thank the reviewers for their insightful comments which lead to the significant improvement in this article.

Declaration of competing interest

No potential conflict of interest was reported by the authors.

Appendix A

Table A.1
Approximate areas and numbers of measurement points for each face and edge.

Face label	Area (m^2)	Point number	Edge label	Area (m^2)	Point number
F1	0.043	353191	Ce1	0.004	38883
F2	0.038	250718	Ce2	0.008	71283
F3	0.023	137471	Ce3	0.005	39114
F4	0.006	33471	Ce4	0.005	49413
F5	0.012	67510	Ce5	0.004	15852
F6	0.050	405301	Ci1	0.008	35267
			Ci2	0.002	8925

Table A.2
Face Flatness error data - precision of mating surfaces.

8 mm Sample: 1						12 mm Sample: 1						16 mm Sample: 1					
Plane	Inclination angle	Maximum error		Mean volume error		Plane	Inclination angle	Maximum error		Mean volume error		Plane	Inclination angle	Maximum error		Mean volume error	
		+ve	−ve	+ve	−ve			+ve	−ve	+ve	−ve			+ve	−ve	+ve	−ve
	(degrees)	(mm)	(mm)	(z - mm)	(z - mm)		(degrees)	(mm)	(mm)	(z - mm)	(z - mm)		(degrees)	(mm)	(mm)	(z - mm)	(z - mm)
F1	30	3.3	−3.5	0.47	−0.47	F1	30	4.5	−6.0	0.53	−0.53	F1	30	4.3	−7.3	0.83	−0.83
F2	45	2.3	−2.6	0.27	−0.27	F2	45	3.4	−4.3	0.42	−0.42	F2	45	4.1	−5.5	0.65	−0.65
F3	60	2.2	−2.5	0.25	−0.25	F3	60	2.9	−5.0	0.54	−0.54	F3	60	3.7	−5.2	0.56	−0.56
F4	90	2.0	−3.0	0.33	−0.33	F4	90	3.8	−6.9	0.83	−0.83	F4	90	3.1	−4.8	0.45	−0.39
F5	90	2.6	−2.6	0.26	−0.26	F5	90	3.0	−4.2	0.46	−0.46	F5	90	2.7	−3.7	0.35	−0.35
F6	0	2.7	−1.3	0.19	−0.19	F6	0	3.7	−2.2	0.20	−0.20	F6	0	2.8	−4.5	0.38	−0.38
8 mm Sample: 2						12 mm Sample: 2						16 mm Sample: 2					
Plane	Inclination angle	Maximum error		Mean volume error		Plane	Inclination angle	Maximum error		Mean volume error		Plane	Inclination angle	Maximum error		Mean volume error	
		+ve	−ve	+ve	−ve			+ve	−ve	+ve	−ve			+ve	−ve	+ve	−ve
	(degrees)	(mm)	(mm)	(z - mm)	(z - mm)		(degrees)	(mm)	(mm)	(z - mm)	(z - mm)		(degrees)	(mm)	(mm)	(z - mm)	(z - mm)
F1	30	2.8	−5.1	0.43	−0.43	F1	30	3.8	−6.4	0.60	−0.60	F1	30	3.9	−6.4	0.77	−0.77
F2	45	3.1	−4.2	0.40	−0.40	F2	45	3.6	−4.3	0.47	−0.47	F2	45	2.9	−4.3	0.54	−0.54
F3	60	3.3	−4.4	0.45	−0.45	F3	60	3.7	−6.3	0.61	−0.61	F3	60	2.8	−4.1	0.48	−0.48
F4	90	4.4	−3.1	0.31	−0.31	F4	90	3.5	−9.3	0.74	−0.74	F4	90	2.6	−3.9	0.46	−0.46
F5	90	4.4	−3.3	0.42	−0.42	F5	90	4.0	−4.8	0.67	−0.67	F5	90	2.7	−2.9	0.36	−0.36
F6	0	2.7	−1.4	0.17	−0.17	F6	0	3.3	−1.9	0.26	−0.26	F6	0	4.2	−2.8	0.34	−0.34

8 mm Sample: 3						12 mm Sample: 3						16 mm Sample: 3					
Plane	Inclination angle	Maximum error		Mean volume error		Plane	Inclination angle	Maximum error		Mean volume error		Plane	Inclination angle	Maximum error		Mean volume error	
		+ve	−ve	+ve	−ve			+ve	−ve	+ve	−ve			+ve	−ve	+ve	−ve
	(degrees)	(mm)	(mm)	(z - mm)	(z - mm)		(degrees)	(mm)	(mm)	(z - mm)	(z - mm)		(degrees)	(mm)	(mm)	(z - mm)	(z - mm)
F1	30	3.6	−4.6	0.44	−0.44	F1	30	3.5	−5.8	0.77	−0.77	F1	30	3.7	−5.9	0.76	−0.76
F2	45	2.3	−2.4	0.28	−0.28	F2	45	3.0	−3.4	0.38	−0.38	F2	45	3.2	−4.3	0.55	−0.55
F3	60	2.0	−3.4	0.33	−0.33	F3	60	2.4	−3.1	0.36	−0.36	F3	60	3.2	−4.0	0.52	−0.52
F4	90	2.3	−3.5	0.33	−0.33	F4	90	3.4	−2.7	0.23	−0.23	F4	90	2.6	−6.3	0.52	−0.52
F5	90	2.4	−3.0	0.34	−0.34	F5	90	2.1	−3.3	0.24	−0.24	F5	90	3.0	−3.3	0.43	−0.43
F6	0	1.7	−1.8	0.24	−0.24	F6	0	3.1	−1.6	0.25	−0.25	F6	0	4.8	−3.0	0.37	−0.37

Table A.3
Edge Profile error data - proximity to the part net-shape.

8 mm Sample: 1						12 mm Sample: 1						16 mm Sample: 1					
Edge	Angle	Maximum error		Mean volume error		Edge	Angle	Maximum error		Mean volume error		Edge	Angle	Maximum error		Mean volume error	
	(x,y)-z1-z2	+ve	−ve	+ve	−ve		(x,y)-z1-z2	+ve	−ve	+ve	−ve		(x,y)-z1-z2	+ve	−ve	+ve	−ve
	(degrees)	(mm)	(mm)	(z - mm)	(z - mm)		(degrees)	(mm)	(mm)	(z - mm)	(z - mm)		(degrees)	(mm)	(mm)	(z - mm)	(z - mm)
Ce1	90-90-30		−5.0		−0.71	Ce1	90-90-30		−4.0		−0.16	Ce1	90-90-30		−8.2		−2.58
Ce2	90-30-45		−6.0		−0.61	Ce2	90-30-45		−7.9		−0.50	Ce2	90-30-45		−12.4		−1.66
Ce3	90-45-60		−3.6		−0.33	Ce3	90-45-60		−7.2		−0.90	Ce3	90-45-60		−8.8		−2.10
Ce4	90-60-90		−2.7		−0.09	Ce4	90-60-90		−0.8		0.00	Ce4	90-60-90		−5.5		−0.28
Ce5	90-90-90		−4.7		−0.81	Ce5	90-90-90		−5.1		−0.40	Ce5	90-90-90		−7.5		−2.44
Ci1	135-90-90	9.1		3.28		Ci1	135-90-90	19.6		6.32		Ci1	135-90-90	11.9		4.75	
Ci2	135-90-90	5.7		0.95		Ci2	135-90-90	9.5		5.08		Ci2	135-90-90	4.0		1.04	
8 mm Sample: 2						12 mm Sample: 2						16 mm Sample: 2					
Edge	Angle	Maximum error		Mean volume error		Edge	Angle	Maximum error		Mean volume error		Edge	Angle	Maximum error		Mean volume error	
	(x,y)-z1-z2	+ve	−ve	+ve	−ve		(x,y)-z1-z2	+ve	−ve	+ve	−ve		(x,y)-z1-z2	+ve	−ve	+ve	−ve
	(degrees)	(mm)	(mm)	(z - mm)	(z - mm)		(degrees)	(mm)	(mm)	(z - mm)	(z - mm)		(degrees)	(mm)	(mm)	(z - mm)	(z - mm)
Ce1	90-90-30		−4.4		−0.83	Ce1	90-90-30		−5.1		−0.36	Ce1	90-90-30		−8.1		−2.38
Ce2	90-30-45		−4.6		−0.50	Ce2	90-30-45		−7.3		−0.55	Ce2	90-30-45		−14.2		−1.89
Ce3	90-45-60		−4.1		−0.56	Ce3	90-45-60		−6.5		−0.87	Ce3	90-45-60		−8.3		−1.36
Ce4	90-60-90		−2.0		0.00	Ce4	90-60-90		−8.5		−0.01	Ce4	90-60-90		−3.4		−0.13
Ce5	90-90-90		−5.9		−1.69	Ce5	90-90-90		−6.4		−1.15	Ce5	90-90-90		−8.2		−2.78
Ci1	135-90-90	9.0		2.66		Ci1	135-90-90	13.6		4.12		Ci1	135-90-90	9.3		3.50	
Ci2	135-90-90	3.7		1.30		Ci2	135-90-90	8.2		4.25		Ci2	135-90-90	3.5		0.83	
8 mm Sample: 3						12 mm Sample: 3						16 mm Sample: 3					
Edge	Angle	Maximum error		Mean volume error		Edge	Angle	Maximum error		Mean volume error		Edge	Angle	Maximum error		Mean volume error	
	(x,y)-z1-z2	+ve	−ve	+ve	−ve		(x,y)-z1-z2	+ve	−ve	+ve	−ve		(x,y)-z1-z2	+ve	−ve	+ve	−ve
	(degrees)	(mm)	(mm)	(z - mm)	(z - mm)		(degrees)	(mm)	(mm)	(z - mm)	(z - mm)		(degrees)	(mm)	(mm)	(z - mm)	(z - mm)
Ce1	90-90-30		−4.4		−0.79	Ce1	90-90-30		−6.0		−1.49	Ce1	90-90-30		−7.7		−2.56
Ce2	90-30-45		−4.7		−0.48	Ce2	90-30-45		−11.3		−1.39	Ce2	90-30-45		−13.0		−2.14
Ce3	90-45-60		−4.6		−0.58	Ce3	90-45-60		−8.4		−1.67	Ce3	90-45-60		−7.6		−1.98
Ce4	90-60-90		−8.3		0.00	Ce4	90-60-90		−3.5		−0.15	Ce4	90-60-90		−3.8		−0.16
Ce5	90-90-90		−4.8		−0.81	Ce5	90-90-90		−8.3		−3.24	Ce5	90-90-90		−8.3		−2.52
Ci1	135-90-90	9.2		2.43		Ci1	135-90-90	8.6		0.92		Ci1	135-90-90	12.4		4.42	
Ci2	135-90-90	3.2		0.91		Ci2	135-90-90	5.8		0.81		Ci2	135-90-90	3.6		0.83	

Note: In 'Angle (x,y)-z1-z2', '(x,y)' represents the edge angle of the toolpath for each layer; 'z1' and 'z2' both represent the horizontal angles of the two flat faces adjacent to the edge.

Table A.4
Face Profile error data - proximity to the part net-shape.

8 mm Sample: 1						12 mm Sample: 1						16 mm Sample: 1					
Plane	Inclination angle	Maximum error		Mean volume error		Plane	Inclination angle	Maximum error		Mean volume error		Plane	Inclination angle	Maximum error		Mean volume error	
		+ve	−ve	+ve	−ve			+ve	−ve	+ve	−ve			+ve	−ve	+ve	−ve
	(degrees)	(mm)	(mm)	(z - mm)	(z - mm)		(degrees)	(mm)	(mm)	(z - mm)	(z - mm)		(degrees)	(mm)	(mm)	(z - mm)	(z - mm)
F1	30	5.0	−4.5	0.47	−0.62	F1	30	5.6	−4.8	1.51	−0.14	F1	30	3.7	−7.3	0.46	−0.99
F2	45	6.7	−2.6	1.50	−0.13	F2	45	5.0	−3.1	1.29	−0.08	F2	45	3.1	−5.5	0.38	−0.83
F3	60	3.5	−3.8	0.22	−0.56	F3	60	7.8	−4.2	2.59	−0.13	F3	60	4.5	−4.6	0.65	−0.45
F4	90	4.7	−1.4	2.21	−0.02	F4	90	7.4	−1.6	3.86	−0.07	F4	90	6.1	−2.6	1.74	−0.07
F5	90	2.8	−3.2	0.21	−0.53	F5	90	6.8	−3.1	2.25	−0.10	F5	90	2.6	−3.2	0.44	−0.19
F6	0	2.2	−1.7	0.03	−0.66	F6	0	4.0	−2.2	0.26	−0.30	F6	0	4.4	−3.0	0.32	−0.44
8 mm Sample: 2						12 mm Sample: 2						16 mm Sample: 2					
Plane	Inclination angle	Maximum error		Mean volume error		Plane	Inclination angle	Maximum error		Mean volume error		Plane	Inclination angle	Maximum error		Mean volume error	
		+ve	−ve	+ve	−ve			+ve	−ve	+ve	−ve			+ve	−ve	+ve	−ve
	(degrees)	(mm)	(mm)	(z - mm)	(z - mm)		(degrees)	(mm)	(mm)	(z - mm)	(z - mm)		(degrees)	(mm)	(mm)	(z - mm)	(z - mm)
F1	30	3.5	−3.6	0.64	−0.29	F1	30	4.7	−5.4	1.27	−0.29	F1	30	3.6	−7.2	0.49	−1.01
F2	45	3.8	−3.0	0.57	−0.26	F2	45	5.0	−3.1	1.34	−0.10	F2	45	4.8	−4.2	1.07	−0.35
F3	60	3.8	−3.5	0.83	−0.29	F3	60	6.5	−4.8	1.38	−0.32	F3	60	4.2	−5.1	1.09	−0.31
F4	90	2.6	−2.7	0.55	−0.29	F4	90	5.8	−2.3	1.63	−0.15	F4	90	4.7	−4.0	1.19	−0.30
F5	90	2.6	−3.3	0.46	−0.68	F5	90	7.1	−3.3	2.23	−0.19	F5	90	2.9	−3.3	0.60	−0.26
F6	0	2.1	−2.4	0.03	−0.66	F6	0	3.1	−2.2	0.23	−0.30	F6	0	5.0	−4.1	0.29	−0.68
8 mm Sample: 3						12 mm Sample: 3						16 mm Sample: 3					
Plane	Inclination angle	Maximum error		Mean volume error		Plane	Inclination angle	Maximum error		Mean volume error		Plane	Inclination angle	Maximum error		Mean volume error	
		+ve	−ve	+ve	−ve			+ve	−ve	+ve	−ve			+ve	−ve	+ve	−ve
	(degrees)	(mm)	(mm)	(z - mm)	(z - mm)		(degrees)	(mm)	(mm)	(z - mm)	(z - mm)		(degrees)	(mm)	(mm)	(z - mm)	(z - mm)
F1	30	4.0	−3.9	0.43	−0.48	F1	30	3.3	−7.1	0.23	−1.38	F1	30	2.9	−7.0	0.46	−1.07
F2	45	3.5	−2.6	0.76	−0.13	F2	45	4.7	−3.9	0.28	−0.76	F2	45	3.4	−4.5	0.61	−0.56
F3	60	3.7	−3.7	0.70	−0.27	F3	60	3.6	−3.5	0.30	−0.51	F3	60	4.3	−4.7	0.90	−0.50
F4	90	3.1	−2.0	0.85	−0.10	F4	90	2.6	−4.5	0.00	−1.18	F4	90	5.9	−5.1	1.32	−0.42
F5	90	2.9	−2.8	0.55	−0.24	F5	90	1.3	−4.1	0.20	−0.97	F5	90	4.2	−3.2	0.93	−0.25
F6	0	1.9	−1.9	0.19	−0.35	F6	0	3.4	−1.5	0.40	−0.15	F6	0	5.4	−3.9	0.31	−0.60

References

[1] N. Labonnote, A. Rønnquist, B. Manum, P. Rüther, Additive construction: state-of-the-art, challenges and opportunities, Autom. Constr. 72 (2016) 347–366, https://doi.org/10.1016/j.autcon.2016.08.026.

[2] D. Ahn, J.H. Kweon, S. Kwon, J. Song, S. Lee, Representation of surface roughness in fused deposition modeling, J. Mater. Process. Technol. 209 (15–16) (2009) 5593–5600, https://doi.org/10.1016/j.jmatprotec.2009.05.016.

[3] R.A. Buswell, W.L. de Silva, S.Z. Jones, J. Dirrenberger, 3D printing using concrete extrusion: a roadmap for research, Cem. Concr. Res. 112 (2018) 37–49, https://doi.org/10.1016/j.cemconres.2018.05.006.

[4] R. de Laubier, M. Wunder, S. Wittoft, C. Rothballer, Will 3D printing remodel the construction industry? The Boston Consulting Group (BCG), Boston, MA, https://image-src.bcg.com/Images/BCG-Will-3D-Printing-Remodel-the-Construction-Industry-Jan-2018_tcm9-181569.pdf, (2018) , Accessed date: 6 April 2020.

[5] J.G. Zhou, D. Herscovici, C.C. Chen, Parametric process optimization to improve the accuracy of rapid prototyped stereolithography parts, Int. J. Mach. Tools Manuf. 40 (3) (2000) 363–379, https://doi.org/10.1016/S0890-6955(99)00068-1.

[6] N.N. Kumbhar, A.V. Mulay, Post processing methods used to improve surface finish of products which are manufactured by additive manufacturing technologies: a review, J. Inst. Eng. (India): Ser. C 99 (4) (2018) 481–487, https://doi.org/10.1007/s40032-016-0340-z.

[7] S. Lim, R.A. Buswell, T.T. Le, R. Wackrow, S.A. Austin, A.G. Gibb, T. Thorpe, Development of a viable concrete printing process, Proceedings of the 28th International Symposium on Automation and Robotics in Construction (ISARC2011), Imperial Palace Hotel, Seoul, South Korea, 2011, pp. 665–670 29 Jun–2 Jul 2011. ISBN: 9781510804296 10.22260/ISARC2011/0124.

[8] B. Khoshnevis, Automated construction by contour crafting—related robotics and information technologies, Autom. Constr. 13 (1) (2004) 5–19, https://doi.org/10.1016/j.autcon.2003.08.012.

[9] F. Bos, R. Wolfs, Z. Ahmed, T. Salet, Additive manufacturing of concrete in construction: potentials and challenges of 3D concrete printing, Virtual Phys. Prototyp. 11 (3) (2016) 209–225, https://doi.org/10.1080/17452759.2016.1209867.

[10] IAAC, Minibuilders, http://robots.iaac.net/, (2014) , Accessed date: 6 April 2020.

[11] Rudenko, Concrete 3D castle, http://www.totalkustom.com/, (2014) , Accessed date: 6 April 2020.

[12] BetAbram, http://www.betabram.com/, (2016) , Accessed date: 6 April 2020.

[13] 3dprint.com, Chinese construction company 3D prints an entire two-story house on-site in 45 days, *https://3dprint.com/138664/huashang-tengda-3d-print-house/*, (2016) , Accessed date: 6 April 2020.

[14] Cnet.com, Dubai unveils world's first 3D-printed office building, https://www.cnet.com/news/dubai-unveils-worlds-first-3d-printed-office-building/, (2016) , Accessed date: 6 April 2020.

[15] S. Lim, R.A. Buswell, P.J. Valentine, D. Piker, S.A. Austin, X. De Kestelier, Modelling curved-layered printing paths for fabricating large-scale construction components, Addit. Manuf. 12 (2016) 216–230, https://doi.org/10.1016/j.addma.2016.06.004.

[16] J. Xu, L. Ding, P.E. Love, Digital reproduction of historical building ornamental components: from 3D scanning to 3D printing, Autom. Constr. 76 (2017) 85–96, https://doi.org/10.1016/j.autcon.2017.01.010.

[17] R.A. Buswell, R.C. Soar, A.G. Gibb, A. Thorpe, Freeform construction: mega-scale rapid manufacturing for construction, Autom. Constr. 16 (2) (2007) 224–231, https://doi.org/10.1016/j.autcon.2006.05.002.

[18] V. Mechtcherine, V.N. Nerella, F. Will, M. Näther, J. Otto, M. Krause, Large-scale

digital concrete construction–CONPrint3D concept for on-site, monolithic 3D-printing, Autom. Constr. 107 (2019) 102933https://doi:10.1016/j.autcon.2019.102933.
[19] B. Khoshnevis, D. Hwang, K.T. Yao, Z. Yeh, Mega-scale fabrication by contour crafting, Int. J. Ind. Syst. Eng. 1 (3) (2006) 301–320, https://doi.org/10.1504/IJISE.2006.009791.
[20] J. Xu, L. Ding, et al., Volume-forming 3D concrete printing using a variable-size square nozzle, Autom. Constr. 104 (2019) 95–106, https://doi.org/10.1016/j.autcon.2019.03.008.
[21] R.J.M. Wolfs, F.P. Bos, T.A.M. Salet, Early age mechanical behaviour of 3D printed concrete: numerical modelling and experimental testing, Cem. Concr. Res. 106 (2018) 103–116, https://doi.org/10.1016/j.cemconres.2018.02.001 (doi:10.1016/j.cemconres.2018.02.001).
[22] A. Perrot, D. Rangeard, A. Pierre, Structural built-up of cement-based materials used for 3D-printing extrusion techniques, Mater. Struct. 49 (4) (2016) 1213–1220, https://doi.org/10.1617/s11527-015-0571-0.
[23] L. Reiter, T. Wangler, N. Roussel, R.J. Flatt, The role of early age structural build-up in digital fabrication with concrete, Cem. Concr. Res. 112 (2018) 86–95, https://doi.org/10.1016/j.cemconres.2018.05.011.
[24] A. Alexandridis, N.J. Gardner, Mechanical behaviour of fresh concrete, Cem. Concr. Res. 11 (3) (1981) 323–339, https://doi.org/10.1016/0008-8846(81)90105-8.
[25] G. Lu, K. Wang, Investigation into yield behavior of fresh cement paste: model and experiment, ACI Mater. J. 107 (1) (2010) 12, https://doi.org/10.14359/51663459.
[26] N. Roussel, Rheological requirements for printable concretes, Cem. Concr. Res. 112 (2018) 76–85, https://doi.org/10.1016/j.cemconres.2018.04.005.
[27] J. Kruger, S. Zeranka, G. van Zijl, 3D concrete printing: a lower bound analytical model for buildability performance quantification, Autom. Constr. 106 (2019) 102904, , https://doi.org/10.1016/j.autcon.2019.102904.
[28] J. Kruger, S. Zeranka, G. van Zijl, Quantifying constructability performance of 3D concrete printing via rheology-based analytical models, in: V. Mechtcherine, K. Khayat, E. Secrieru (Eds.), Rheology and Processing of Construction Materials. RheoCon 2019, SCC 2019, RILEM Bookseries, 23 Springer, Cham, 2020, , https://doi.org/10.1007/978-3-030-22566-7_46.
[29] A.S.J. Suiker, Mechanical performance of wall structures in 3D printing processes: theory, design tools and experiments, Int. J. Mech. Sci. 137 (2018) 145–170, https://doi.org/10.1016/j.ijmecsci.2018.01.010.
[30] R.J.M. Wolfs, A.S.J. Suiker, Structural failure during extrusion-based 3D printing processes, Int. J. Adv. Manuf. Technol. (2019) 1–20, https://doi.org/10.1007/s00170-019-03844-6.
[31] J. Campbell, The concept of net shape for castings, Mater. Des. 21 (4) (2000) 373–380, https://doi.org/10.1016/S0261-3069(99)00072-2.
[32] D.K. Ballast, Handbook of Construction Tolerances, John Wiley & Sons, New York, 2007 ISBN: 978-0-471-93151-5 (cloth).
[33] CII, Constructability Implementation Guide, second edition, CII Special Publication vols. 34-1, The University of Texas at Austin, Austin, Texas, 2006https://www.construction-institute.org/resources/knowledgebase/best-practices/constructability/topics/rt-034/pubs/sp34-1# , Accessed date: 6 April 2020.
[34] H.B. Voelcker, Dimensional tolerancing today, tomorrow, and beyond, Advanced Tolerancing Techniques, John Wiley & Sons, New York, 1997, pp. 3–12 (ISBN: 978-0-471-14594-3).
[35] C.T. Milberg, Application of tolerance management to civil systems, Doctoral dissertation University of California, Berkeley, http://citeseerx.ist.psu.edu/viewdoc/download?doi=10.1.1.308.5119&rep=rep1&type=pdf, (2006) , Accessed date: 6 April 2020.
[36] J.G. Everett, A.H. Slocum, Automation and robotics opportunities: construction versus manufacturing, J. Constr. Eng. Manag. 120 (2) (1994) 443–452, https://doi.org/10.1061/(ASCE)0733-9364(1994)120:2(443).
[37] G.R. Cogorno, Geometric Dimensioning and Tolerancing for Mechanical Design, McGraw-Hill, 2017, https://doi.org/10.1036/0071460705.
[38] BSI, Newly revised BS 8888:2006 technical product specification, https://www.bsigroup.com/en-GB/about-bsi/media-centre/press-releases/2007/1/Newly-Revised-BS-8888-2006-Technical-Product-Specification/ , Accessed date: 6 April 2020.
[39] ASME, Y14.5, https://www.asme.org/products/codes-standards/y145-2018-dimensioning-and-tolerancing, (2018) , Accessed date: 6 April 2020.
[40] G. Henzold, https://vufind.lboro.ac.uk/Record/436752, (2006) , Accessed date: 6 April 2020.
[41] GB/T 1182-2018, http://111.203.12.48/bzgk/gb/newGbInfo?hcno=C87A687A21B36E2F2D3A09BDF03DCA01 , Accessed date: 6 April 2020.
[42] C. Milberg, I. Tommelein, Role of tolerances and process capability data in product and process design integration, Proceedings of Construction Research Congress, 8 ASCE, Honolulu, Hawaii, 2003, March, , https://doi.org/10.1061/40671(2003)93.
[43] C.C. Tsao, I.D. Tommelein, E.S. Swanlund, G.A. Howell, Work structuring to achieve integrated product–process design, J. Constr. Eng. Manag. 130 (6) (2004) 780–789, https://doi.org/10.1061/(ASCE)0733-9364(2004)130:6(780).
[44] S.Y. Lam, Application of terrestrial laser scanning methodology in geometric tolerances analysis of tunnel structures, Tunn. Undergr. Space Technol. 21 (3) (2006) 410, https://doi.org/10.1016/j.tust.2005.12.057.
[45] Construction 2025: strategy, https://www.gov.uk/government/publications/construction-2025-strategy , Accessed date: 6 April 2020.
[46] Strategy for the sustainable competitiveness of the construction sector and its enterprises, https://eur-lex.europa.eu/legal-content/EN/TXT/?uri=CELEX:52012DC0433 , Accessed date: 6 April 2020.
[47] J. Xu, R. Buswell, P. Kinnell, Test Part CAD Model for GD&T in 3D Concrete Printing.STL. Figshare, Online resource (2020), https://doi.org/10.17028/rd.lboro.11536614.v1.
[48] T.T. Le, S.A. Austin, S. Lim, R.A. Buswell, A.G. Gibb, T. Thorpe, Mix design and fresh properties for high-performance printing concrete, Mater. Struct. 45 (8) (2012) 1221–1232, https://doi.org/10.1617/s11527-012-9828-z.
[49] Simplyfy3D, Software features, https://www.simplify3d.com/software/features/, (2018) , Accessed date: 6 April 2020.
[50] I. Moring, H. Ailisto, V. Koivunen, R. Myllylä, Active 3-D vision system for automatic model-based shape inspection, Opt. Lasers Eng. 10 (3–4) (1989) 149–160, https://doi.org/10.1016/0143-8166(89)90034-1.
[51] Z. Ji, M.C. Leu, Design of optical triangulation devices, Opt. Laser Technol. 21 (5) (1989) 339–341, https://doi.org/10.1016/0030-3992(89)90068-6.
[52] Y. Yu, T. Kondo, T. Ohyama, T. Honda, J. Tsujiuchi, Measuring gear tooth surface error by fringe scanning interferometry, Acta Metrol. Sin. 9 (2) (1988) 120–123 http://new.oversea.cnki.net/ , Accessed date: 6 April 2020.
[53] W. Wester-Ebbinghaus, Analytics in non-topographic photogrammetry, Proceedings of the XVIth ISPRS Congress, Commission V, Kyoto, Japan, 1–10 July 1988, XXVII International Society for Photogrammetry and Remote Sensing, 1988, pp. 380–392 Part B5 https://www.isprs.org/proceedings/XXVII/congress/part5/380_XXVII-part5-sup.pdf , Accessed date: 6 April 2020.
[54] W. Schertenleib, Measurement of structures (surfaces) utilizing the smart 310 laser-tracking-system, KEK Proceedings, National Laboratory for High Energy Physics, 1995, pp. III–251 https://www-group.slac.stanford.edu/met/IWAA/TOC_S/Papers/WSche95.pdf , Accessed date: 6 April 2020.
[55] V. Srinivasan, H.C. Liu, M. Halioua, Automated phase-measuring profilometry of 3-D diffuse objects, Appl. Opt. 23 (18) (1984) 3105–3108, https://doi.org/10.1364/AO.23.003105.
[56] J.A. Jalkio, R.C. Kim, S.K. Case, Three dimensional inspection using multistripe structured light, Opt. Eng. 24 (6) (1985) 246966, https://doi.org/10.1117/12.7973609.
[57] F. Chen, G.M. Brown, M. Song, Overview of 3-D shape measurement using optical methods, Opt. Eng. (2000) 39, https://doi.org/10.1117/1.602438.
[58] HP, HP 3D scan brilliantly capture reality, http://www8.hp.com/us/en/campaign/3Dscanner/overview.html?jumpid=va_t1345uf8k6, (2018) , Accessed date: 6 April 2020.
[59] S. Seeger, X. Laboureux, Feature extraction and registration: an overview, Principles of 3D Image Analysis and Synthesis, 2002, pp. 153–166, , https://doi.org/10.1007/978-1-4757-3186-6.
[60] P.J. Besl, N.D. McKay, Method for registration of 3-D shapes, Sensor Fusion IV: Control Paradigms and Data Structures, 1611 International Society for Optics and Photonics, 1992, April, pp. 586–607, , https://doi.org/10.1117/12.57955.
[61] A. Mandow, J.L. Martínez, A.J. Reina, J. Morales, Fast range-independent spherical subsampling of 3D laser scanner points and data reduction performance evaluation for scene registration, Pattern Recogn. Lett. 31 (11) (2010) 1239–1250, https://doi.org/10.1016/j.patrec.2010.03.008.
[62] F.H. Wittmann (Ed.), Fundamental Research on Creep and Shrinkage of Concrete, Springer Science & Business Media, 2012, , https://doi.org/10.1007/978-94-010-3716-7 ISBN-13:978-94-010-3718-1.
[63] P. Kinnell, T. Rymer, J. Hodgson, L. Justham, M. Jackson, Autonomous metrology for robot mounted 3D vision systems, CIRP Ann. 66 (1) (2017) 483–486, https://doi.org/10.1016/j.cirp.2017.04.069.
[64] J.R. Hodgson, P. Kinnell, L. Justham, N. Lohse, M.R. Jackson, Novel metrics and methodology for the characterisation of 3D imaging systems, Opt. Lasers Eng. 91 (2017) 169–177, https://doi.org/10.1016/j.optlaseng.2016.11.007.